Bone 206 (2026) 117814

Contents lists available at ScienceDirect

Bone

journal homepage: www.elsevier.com/locate/bone

Full Length Article

Activin-A has dual roles in osteoclast formation and foreign body giant cell differentiation from human CD14^{+} monocytes

Elina Kylmäoja [a], Sami Kauppinen [b,g], Faleh Abushahba [c,d], Mikko Finnilä [b,g], Mikko Ritala [e], Petri Lehenkari [a], Juha Tuukkanen [a], Teun J. de Vries [f], Ton Schoenmaker [f,*]

[a] Research Unit of Translational Medicine, Department of Anatomy and Cell Biology, Medical Research Center, P.O. Box 5000, 90014, University of Oulu, Oulu, Finland
[b] Research Unit of Health Sciences and Technology, Faculty of Medicine, University of Oulu, Finland
[c] Department of Prosthetic Dentistry and Stomatognathic Physiology, Institute of Dentistry, University of Turku, Turku, Finland
[d] Department of Biomaterials Science and Turku Clinical Biomaterials Center—TCBC, Institute of Dentistry, University of Turku, Turku, Finland
[e] Department of Chemistry, University of Helsinki, P.O. Box 55, 00014, Helsinki, Finland
[f] Department of Periodontology, Academic Centre for Dentistry Amsterdam (ACTA), University of Amsterdam and Vrije Universiteit Amsterdam, Amsterdam Movement Sciences, Amsterdam, the Netherlands
[g] Biocenter Oulu, University of Oulu, Oulu, Finland

ARTICLE INFO

Keywords:
Osteoclast
Foreign body giant cell
Activin A
Biomaterials

ABSTRACT

Osteoclasts and foreign body giant cells (FBGCs) are multinucleated cells derived from monocytes, but they have distinct functions. Osteoclasts resorb bone while FBGCs form in response to foreign material. Regarding bone implants, osteoclasts are responsible for implant integration, but also for bone resorption associated to implant loosening, while FBGCs play a role in the immune response to the foreign material. Little is known about which proteins in the local environment fine-tune the multinucleation of osteoclasts or FBGCs. One candidate is Activin A (ActA). It has been shown to induce larger, more active osteoclasts, but its effect on FBGC differentiation is unknown.

We investigated the effect of ActA on the differentiation of osteoclasts and FBGCs from human CD14-positive monocytes. The number of multinucleated cells and the cell area was measured. qPCR was performed to assess the effect of ActA on gene expression. ActA's influence on osteoclast and FBGC formation was studied on plastic, bone and hydroxyapatite coated Titanium discs (ALD-HA).

ActA induced fewer, but bigger and more active osteoclasts on plastic and bone. In contrast, ActA did not have an effect on FBGC number. On ALD-HA, ActA reduced the number of FBGCs, but did not influence osteoclast numbers. qPCR showed that ActA upregulated the expression of several genes such as TRAcP, CIITA, OLR1, RHOBTB1 and ALK4, but mainly in osteoclasts. These results show that ActA has a different effect on osteoclasts compared to FBGCs. This difference could be caused by a difference in the expression in the canonical ActA receptor ALK4.

1. Introduction

Monocytes have the capacity to fuse into two different types of multinucleated cells: osteoclasts, the specialized bone-degrading cells, and foreign body giant cells (FBGC) in response to a foreign material implanted into the body [1]. These two multinucleated cells have many similar properties, but there are also different functional mechanisms that these cells exploit [2–8] as described below.

Osteoclasts are the only cells capable of resorbing bone. The formation of osteoclasts takes place on bone surfaces whenever bone remodeling activity is required. Remodeling is orchestrated by communication between bone cells and includes the degradation of old or weak bone by osteoclasts and the subsequent osteoid formation by osteoblasts, which finally mineralizes this new bone matrix. During this process, some become embedded into the matrix as osteocytes. Osteoclasts are specialized in the resorption of the bone matrix by secretion of

* Corresponding author.
E-mail addresses: elina.kylmaoja@oulu.fi (E. Kylmäoja), sami.kauppinen@oulu.fi (S. Kauppinen), fafabu@utu.fi (F. Abushahba), mikko.finnila@oulu.fi (M. Finnilä), petri.lehenkari@oulu.fi (P. Lehenkari), kjuhak.tuukkanen@gmail.com (J. Tuukkanen), teun.devries@acta.nl (T.J. de Vries), t.schoenmaker@acta.nl (T. Schoenmaker).

https://doi.org/10.1016/j.bone.2026.117814
Received 7 November 2025; Received in revised form 26 January 2026; Accepted 28 January 2026
Available online 4 February 2026

hydrochloric acid for the degradation of the inorganic bone mineral and proteolytic enzymes such as cathepsin K for the degradation of the organic matrix [9,10].

FBGCs cannot resorb bone. Instead they are involved in the foreign body response that occurs when foreign material enters the body. FBGCs differentiate from monocytes around foreign materials as the body's attempt to eliminate or neutralize the foreign substance [11]. However, although FBGCs can be large cells with hundreds of nuclei, they are not necessarily capable of totally degrading the foreign material. FBGCs can secrete reactive oxygen species (ROS) and matrix metalloproteases (MMPs) in attempting to degrade the foreign material, or they can try to phagocytose it [1,5]. The main difference between osteoclasts and FBGCs is that FBGCs are not able to resorb bone, although they are able to dissolve the bone mineral hydroxyapatite-like calcium phosphate coating to some extent, but not as efficiently as osteoclasts [3,12].

For optimal osseointegration of bone implants, it is desirable to have an initial phase of osteoclast formation. Bone that is damaged during the procedure of placing the implant should be remodeled by osteoclasts, followed by activation of osteoblasts [13–15]. In this process, the FBGCs can potentially delay optimal osseointegration. FBGCs are present around implant failures [16] and can therefore be considered as an undesired response [17–19]. Whenever a foreign material is implanted anywhere in the body, a foreign body response is elicited [17]. This is characterized as a series of host responses aimed at eliminating the foreign substance or adapting to its presence. The initial foreign body reaction includes an acute inflammatory reaction. The inflammatory reaction involves the migration of inflammatory cells, such as neutrophils, monocytes and lymphocytes, which produce various regulatory substances including cytokines, growth factors and other bioactive agents [17,19]. If the regulation of the inflammatory reaction is imbalanced, monocyte fusion into FBGCs increases in various tissues, whereas in bone, also osteoclast formation is enhanced, leading to excess inflammation, increased bone resorption and finally to implant loosening [16,18].

It is clinically desirable to know the molecules that affect multinucleation and the activity of osteoclasts and FBGCs. With this knowledge, one can manipulate the formation of either osteoclasts or FBGCs. Activin A (ActA) is one such candidate. It is a TGF-β superfamily protein involved in many physiological reactions [20]. ActA signaling is based on its binding to one of the two cell surface type II receptors (ActRIIA or ActRIIB), which induces a signaling cascade via the ALK4 or ALK7 type I BMP receptors through SMAD2/3 signaling, leading to regulation of cell proliferation, differentiation, metabolism, or apoptosis. In addition to regulatory roles in several other tissues, ActA is expressed by osteoblasts and osteoclasts and has been shown to have either stimulatory or inhibitory effects on bone cells and their differentiation [20–33]. ActA plays a role in inflammation [34,35] and can be produced by and can affect many types of immune cells such as monocytes, macrophages and lymphocytes, and has either anti- or proinflammatory outcomes [36–42]. We have previously shown that ActA decreases the number of osteoclasts but increases the size and activity of osteoclasts differentiated from human $CD14^+$ monocytes [43,44]. It also induces differential expression of more than 1000 genes in these cells belonging to pathways related to differentiation, fusion and inflammation [45].

Since the effects of ActA on FBGC differentiation are not known, it could well be a potential target that acts differently on these two cell types.

To date, titanium (Ti) is still an extensively used bone implant biomaterial, with proven successful osseointegration. The increasing demand for orthopedic implants [46] has driven the development of titanium-based materials that offer superior biocompatibility, strength, and longevity. Atomic layer deposited hydroxyapatite (ALD-HA) on titanium (Ti) has shown promising results in regard to cell attachment and viability [47–49]. ALD is a beneficial coating method for improving osseointegration of Ti implants, as it can provide a uniform, nanoscale coating for complex three-dimensional structures such as bone screws [50,51]. Other coating methods can possess several problems such as cracking and flaking [52–54], but with ALD these problems do not occur.

Both osteoclasts and FBGCs respond to inflammation [1]. To place ActA in the biological context of both osteoclasts and FBGCs, the effect of ActA was studied on both bone and ALD-HA Ti. With regard to bone implants and the foreign body reaction, the different possible effects of ActA on these different cells could provide a mechanism to specifically control the functions of these cells at the implantation site to achieve the optimal osseointegration of the implant. Therefore, we extended the study of the effects of ActA also on ALD-HA Ti to investigate the differentiation of multinucleated cells on this bone implant material, as it represents the clinical application in which understanding the behavior of these cells is particularly critical for successful osseointegration and long-term implant stability.

Since osteoclasts and FBGCs share many properties, but on the contrary have different mechanisms of function, we hypothesized that the effect of ActA on the differentiation of multinucleated cells could have different outcomes in these two cell cultures on the different substrates.

2. Materials and methods

2.1. Preparation of nanocrystalline HA coating (ALD-HA) on Ti substrates with the ALD method

The HA coatings were fabricated on Ti substrates as described by Holopainen et al. [55]. The substrate for the ALD-HA coating was a 5 cm × 5 cm (25 cm^2), 1 mm thick titanium sheet (Grade 2, ASTM B265 specification, William Gregor Ltd., London, UK). The ALD coating was started by depositing a thin film of $CaCO_3$ in an F-120 ALD reactor (ASM Microchemistry Ltd., Helsinki, Finland) with nitrogen carrier and purging gas. The $CaCO_3$ films were deposited using the $Ca(thd)_2$—O_3 process previously reported in the literature [56]. $Ca(thd)_2$ (Volatec Oy, Vantaa, Finland) was evaporated at 188 °C, and O_3 was generated from O_2 (99.9999%) with a Wedeco Ozomatic Modular 4 HC Lab ozone generator. Samples were produced with 4000 ALD cycles resulting in a thickness of 380 nm. Pulses and purges of 1 s were used for all precursors. The depositions were conducted at 250 °C. Conversion of $CaCO_3$ to HA was achieved by using 0.2 M $(NH_4)_2HPO_4$ (99%; Merck KGaA, Darmstadt, Germany) solution at 95 °C. After conversion, the samples were rinsed with deionized water and blown dry with compressed air. A manual plate cutter (Bernardo PTS 1050 S Manual disc cutter, Linz, Austria) was used for cutting the ALD-coated titanium plates. The Ti plate was firmly placed in a disc pressing to keep it in place during the cutting process. The plate was cut to produce 0.3 × 0.3 cm (0.09 cm^2) square-shaped discs. Before cell culture, the samples were soaked in 70% ethanol for 10 min and air-dried.

2.2. Cell culture and analysis

2.2.1. $CD14^+$ cell isolation

Buffy coats containing peripheral mononuclear cells (PBMCs) were purchased from the Dutch blood bank (Sanquin, Amsterdam, The Netherlands) Permission to use buffy coats to isolate PBMCs for the purpose of osteoclast formation was granted by Sanquin (number: NVT230.0). PBMCs were isolated using Ficoll-Paque density gradient centrifugation. All experiments were performed in accordance with the Declaration of Helsinki. The buffy coats were diluted 1:1 with a 1% PBS-citrate buffer consisting of sodium citrate-2 (1.55 M), citric acid-1 (0.11 M) and phosphate-buffered saline (PBS). 25 ml of diluted blood was carefully layered on 15 ml Lymphoprep (Axisschield Po CAS, Oslo, Norway) and centrifuged at 800 ×*g* during 30 min without braking. After centrifugation, the interphase containing the PBMCs was collected. The PBMCs were centrifuged for 10 min at 400 ×*g* (with brake). Supernatant was decanted and cells were resuspended in the PBS-citrate

buffer. This washing step was repeated 3 times. After the washing steps, cells were resuspended in 20 ml of MACS buffer, consisting of PBS, 0.5% bovine serum albumin (BSA), and 2 mM ethylenediaminetetraacetic acid (EDTA) and counted with a Muse Cell Analyzer (Merck Millipore, Billerica, MA). The cell number was determined and the cells were centrifuged for 10 min at 400 ×*g* (with brake). The supernatant was aspirated and the PBMCs were resuspended in 80 μl of buffer per 10^7 cells. A manual magnetic-assisted cell sorter (MACS) and iron-conjugated CD14 antibodies (Miltenyi Biotec, Bergisch Gladbach, Germany) were used to isolate $CD14^+$ cells. Per 10^7 cells, 2 μl of CD14 microbeads was added and incubated for 15 min in the refrigerator (2–8 °C) according to the manufacturer's instructions (Miltenyi Biotec). After 15 min of labeling with anti-CD14 beads, cells were washed once and resuspended in 500 μl of buffer. Subsequently the PBMC suspension was applied to the magnetic column. The column was rinsed 3× with 3 ml MACS buffer, allowing non-labeled cells to come off the column. Next, the column was removed from the magnet and 5 ml buffer was added to collect the $CD14^+$ cells. The cell density was determined with the Muse Cell Analyzer and after collection of the appropriate number of $CD14^+$ cells, the cells were resuspended in culture medium. The culture medium consisted of alpha minimum essential medium (αMEM; Life Technologies, Carlsbad, CA), 10% fetal calf serum (FCS; HyClone, Logan, UT) and 1% penicillin/streptomycin/fungisone (PSF; Sigma-Aldrich, Saint Louis, MO).

2.2.2. Cell culture

Purified $CD14^+$ cells were suspended in culture medium and were seeded on ALD-HA samples, bovine cortical bone slices or plastic in a final cell concentration of 1×10^5 cells per 0.32 cm^2 (surface of one well). The cells were cultured for 3 days with 25 ng/ml human recombinant macrophage colony-stimulating factor (M-CSF) (R&D Systems, MI) without or with 50 ng/ml Activin-A (Sigma). After 3 days, the concentration of M-CSF was reduced to 10 ng/ml for both FBGC and osteoclast cultures until the end of the culture period. For the generation of FBGCs, 5 ng/ml human recombinant IL-4 and 5 ng/ml human recombinant IL-13 were added to the cultures. For the generation of osteoclasts, 5 ng/ml mouse recombinant RANK-L (R&D Systems) was added. The cell density and the cytokine concentration for the generation of FBGCs and osteoclasts were carefully titrated previously [3]. The culture medium was refreshed every 3–4 days. The total culture time lasted for 14 and 21 days.

2.2.3. Detection of cellular TRAcP activity

After 14 and 21 days the osteoclasts and FBGCs were fixed for 10 min with 4% PBS buffered formaldehyde. The cells on plastic and bone were stained for TRAcP activity (acid phosphatase leukocyte kit; Sigma-Aldrich) according to the manufacturer's protocol, and the nuclei were stained with 4′,6-diamidino-2-fenylindool phenylindole (DAPI; Merck, Whitehouse Station, NJ, USA) in PBS (1:200).

2.2.4. Counting of multinucleated cells on plastic and measurement of cell area

The cells were imaged using a Leica DMIL microscope at 20× magnification and micropgraphs were taken with a digital camera (Leica, Wetzlar, Germany). The number of multinucleated cells was counted from 8 images per well using QuPath image analysis software v0.5.1 [57]. The multinucleated cells were categorized into one of the following three groups: 3 to 5 nuclei per cell, 6 to 10 nuclei per cell and more than 10 nuclei per cell. Cell areas were measured with QuPath by drawing the multinucleated cell outlines by hand and using the annotation measurement tool to obtain the cell areas. All multinucleated cells per image were measured.

2.2.5. Counting of multinucleated cells on ALD-HA

The actin cytoskeleton was stained with Alexa 488-conjugated phalloidin (200 U/ml stock diluted 1:100 in PBS; Invitrogen Europe, Paisley, UK) for 20 min at +37 °C. Nuclei were stained with Hoechst 33258 (1 mg/ml stock diluted 1:800 in PBS; Sigma-Aldrich) for 10 min at RT. The samples were mounted in 70% glycerol-PBS. The cells were imaged using a Zeiss Axio Scope.A1 fluorescence microscope (Oberkochen, Germany) and EC Plan Neofluar 40× objective. Pictures were taken with a digital QImaging MicroPublisher 5.0 RTV camera and QCapture 2.90.1 software (QImaging, Surrey, Canada). The number of multinucleated cells was counted from 5 images per sample using QuPath image analysis software v0.5.1 (Bankhead 2017) by categorizing the cells according to the number of nuclei as in the plastic cell culture analysis.

2.2.6. Confocal microscopy

The actin cytoskeleton was stained with Alexa 488-conjugated phalloidin (200 U/ml stock diluted 1:100 in PBS; Invitrogen Europe, Paisley, UK) for 20 min at +37 °C. Nuclei were stained with Hoechst 33258 (1 mg/ml stock diluted 1:800 in PBS; Sigma-Aldrich) for 10 min at RT. Bone slices and ALD-HA samples were mounted in 70% glycerol-PBS. The cells were viewed with Leica TCS SP8 confocal with a DMI8 microscope using LAS X 3.5.7 acquisition software. The used objective was an HC PL APO CS2 20×/0.75 DRY. Samples were imaged with 499 nm and 405 nm solid-state lasers; the pinhole was set to Airy 0.88 and the scan speed to 600 Hz. The image pixel size was 0.568 μm. Maximum intensity projections (MIPs) were created from the *Z*-stacks.

2.2.7. Field emission scanning electron microscopy (FESEM)

Cells were removed from bone slices with a soft brush. The bone slices and ALD-HA samples were dehydrated in an ascending ethanol series and dried with a critical point drying equipment K850 (Quorum Technologies, Lewes, UK). Samples were coated with 5 nm platinum by Q150T ES sputter coater (Quorum Technologies, Lewes, UK) and viewed with Sigma HD VP FE-SEM (Carl Zeiss Microscopy GmbH, Oberkochen, Germany). FESEM images were taken with 5.0 kV voltage.

2.3. Measurement of resorption pit areas

Resorption pit analysis was conducted using 3D X-ray microscopy (Zeiss Xradia Versa 620). Bone samples were scanned using the following parameters: voltage: 60 kV, power: 6.5 W, filter: Zeiss low energy #2, 2401 projections per 360°, 4× objective, variable exposure time ranging from 1.5 s (short edge) to 3 s (long edge), total scan time of 2 h and 31 min, and a pixel size of 2.79 μm. The data were automatically reconstructed into image stacks using consistent reconstruction settings across all samples. A built-in noise reduction filter (Zeiss NRF) was applied, which was calibrated from the average background noise in the initial scan set ($n = 8$), and uniformly applied to all subsequent scans. All analyses were conducted on 8-bit image data.

Resorption pits were analyzed with modified MATLAB algorithm originally developed for surface roughness analysis. The datasets were first automatically oriented by detecting the sample surface and applying a 3D rotation to align this surface flat in the x–y plane. An automatic region of interest (ROI) was then created by identifying sample edges and fitting a circular mask centered on the dataset. The circle's radius was defined as the distance from the center to the nearest edge, reduced by 5% to minimize edge artifacts. The resulting image stack was saved for downstream analysis.

For resorption pit identification, the data were first binarized using Otsu thresholding [58], retaining only the largest contiguous binary object. The sample surface was then extracted by identifying the first non-zero pixel along the image stack's depth axis, yielding a surface heightmap representing the surface with possible resorption. A 3D baseline surface was generated using the gridfit algorithm [59] and subtracted from the original surface to flatten the baseline. A first-degree polynomial surface was subsequently fitted and shifted 2 pixels (5 μm) downward. Data above this new reference surface were considered non-resorbed, while the remaining data contained resorption pits, osteocyte

lacunae, sawing artifacts, and vascular channels.

To isolate resorption pits, the algorithm excluded features exceeding 50 μm in depth (vascular channels), smaller than 25 μm × 25 μm in area (osteocyte lacunae), or occupying more than 2% of the analysis area (sawing-related artifacts). The depths of the remaining pits were adjusted by re-adding the 5 μm offset. The percentage of resorbed area was subsequently calculated as an area ratio. Resultant images illustrating the analyzed features were generated automatically (Fig. 4B).

2.4. RNA isolation and real time quantitative polymerase chain reaction (qPCR)

For RNA isolation, cells were cultured on plastic for 7, 14 and 21 days and on bone and ALD for 7 days in 96 well plates. For each experimental condition, 2 wells were pooled. RNA from the plastic samples was isolated using the RNeasy mini kit (QIAGEN, Hilden, Germany) following the manufacturer's instructions. For the samples on bone and ALD the Trizol method was used for RNA isolation. cDNA synthesis was performed using the first-strand cDNA synthesis kit (Thermo Fisher Scientific) according to the manufacturer's protocol, using both the Oligo(dT) 18 and the D(N)6 primers.

qPCR was performed on the LC480 light cycler (Roche, Basel, Switzerland). 3 ng cDNA was used in a total volume of 20 μl containing Light Cycler SybrGreen1 Master mix (Roche) and 1 μM of each primer. A standard two-step qPCR program with an annealing temperature of 60 °C was performed, followed by a melting curve analysis to ensure only one product was amplified. To assess efficiencies of the PCR reactions, a standard curve was prepared by serial dilutions of a positive control cDNA sample. To avoid amplification of genomic DNA, each amplicon spanned at least one intron. Sequence information for all primers is listed in Table 1. Expression of housekeeping gene Beta2 Microglobulin (*B2M*) was not affected by the experimental conditions. Samples were normalized for the expression of *B2M* by calculating the ΔCt ($Ct_{,gene\ of\ interest}$ - $Ct_{,B2M}$). Subsequently the ^^Ct was calculated by subtracting the average Ct value of the osteoclast $t = 7$ plastic samples from all other Ct values. Finally, relative expression of the different genes was expressed as $2^{-(\Delta\ \Delta\ Ct)}$. All qPCRs had equal efficiencies.

2.5. Statistical analysis

All experiments were done with duplicate technical replicates. For the number of multinucleated cells and for the qPCR analysis on plastic data were obtained from 8 independent donors. For the cell area measurements on plastic and all experiments on bone and ALD-HA data were obtained from 4 independent donors.

Statistical analyses were performed using GraphpadPrism v10.4.1 (GraphPad, La Jolla, CA, USA). Statistical differences were tested using a 2-way ANOVA followed by Tukey's multiple comparisons test. For the area measurements, paired *t*-tests were performed. $p < 0.05$ was considered significant. Data are shown as means ± SEM.

3. Results

3.1. Acta induces fewer but larger osteoclasts, but does not influence the number of FBGCs

TRAcP-positive multinucleated cells were observed in both osteoclast and FBGC cultures, without or with ActA at both time points 14 and 21 days (Fig. 1A). The intensity of the TRAcP-staining was stronger after 21 days of culture in both cell types. In osteoclast control cultures, the multinucleated cells were mostly small, 3–5 nucleated cells. At both day 14 and 21, ActA decreased the total number of osteoclasts ($p < 0.05$ and $p < 0.01$, respectively; Fig. 1 B & D). When analysing the size of osteoclasts as indicated by the number of nuclei, this decrease in the total number of osteoclasts was due to the significant decrease of the smaller (3–5 nuclei) osteoclasts (Fig. 1 B & D and Fig. S1 A). Supplementary Fig. S1 represents the data of Fig. 1 in separate groups for a detailed comparison between the groups based on the categories of the cells by the number of nuclei (small multinucleated cells with 3–5 nuclei, Fig. S1A and E, intermediate with 6–10 nuclei, Fig. S1 B and F, large with >10 nuclei, Fig. S1 C and G and the total number of multinucleated cells, Fig. S1 D and H) to facilitate the comparison between the osteoclast and FBGC cultures. Osteoclast cultures contained a small number of intermediate-sized or large cells with 6–10 nuclei or >10 nuclei, and ActA did not affect the number of these cells at day 14 or 21.

Regarding FBGC cultures, ActA had no effect on either the small (3–5 nuclei), intermediate-sized (6–10 nuclei) or large (>10 nuclei) multinucleated cell number at the time points studied (Fig. 1 C & E). The main difference in osteoclast and FBGC cultures was observed at day 21 in the bigger cells, as there were significantly more cells with >10 nuclei in the FBGC compared to the osteoclast cultures indicating that FBGCs were generally bigger regardless of the presence of ActA ($p < 0.05$; Fig. S1 G). In contrast, the total number of multinucleated cells was significantly smaller at day 21 in the FBGC group without ActA ($p < 0.05$; Fig. S1 H), suggesting that the smaller cells contribute to a greater extent in this experimental condition.

3.2. Acta increases the multinucleated cell area in osteoclast cultures, but not in FBGC cultures

The cell area analysis after 14 days showed that ActA tends to increase the average area of multinucleated cells in osteoclast cultures (from approximately 2000 to 4000 μm^2) and to decrease the area in the FBGC cultures (from approximately 7500 to 5000 μm^2), but these

Table 1
Primer sequences used for quantitative PCR.

Genes	Oligonucleotide sequence 5′-3′	Amplicon length (bp)	ENSEMBL ID
B2M	AGCTGTGCTCGCGCTACTCTC CACACGGCAGGCATACTCATC	286	ENSG00000166710
TRAcP	CACAATCTGCAGTACCTGCAAgAT CCCATAGTGGAAGCGCAgATA	128	ENSG00000102575
CIITA	GCTCTACTCAGAACCCGACACA TCACACAACAGCCTGCTGAAC	63	ENSG00000179583
OLR1	CCAGCCTGATGAGAAGTCAAATG AGGCACCACCATGGAGAGTAA	72	ENSG00000173391
RHOBTB1	CAGTGTATGCTCCAAGTTCCGTAA CGGTGCCGCTCGAAGTATT	75	ENSG00000072422
ALK4	TGCAGTCACTGACACCATTG CATGGACTCCTCCAGAATTG	188	ENSG00000135503
DCSTAMP	ATTTTCTCAGTGAGCAAGCAGTTTC AGAATCATGGATAATATCTTGAGTTCCTT	101	ENSG00000164935

B2M, β2-microglobulin; *TRAcP*, tartrate resistant acid phosphatase; *CIITA*, class II major histocompatibility complex transactivator; *OLR1*, oxidized low density lipoprotein receptor 1; *RHOBTB1*, Rho related BTB domain containing 1; *ALK4*, Activin A receptor type 1B; *DCSTAMP*, dendritic cell-specific transmembrane protein.

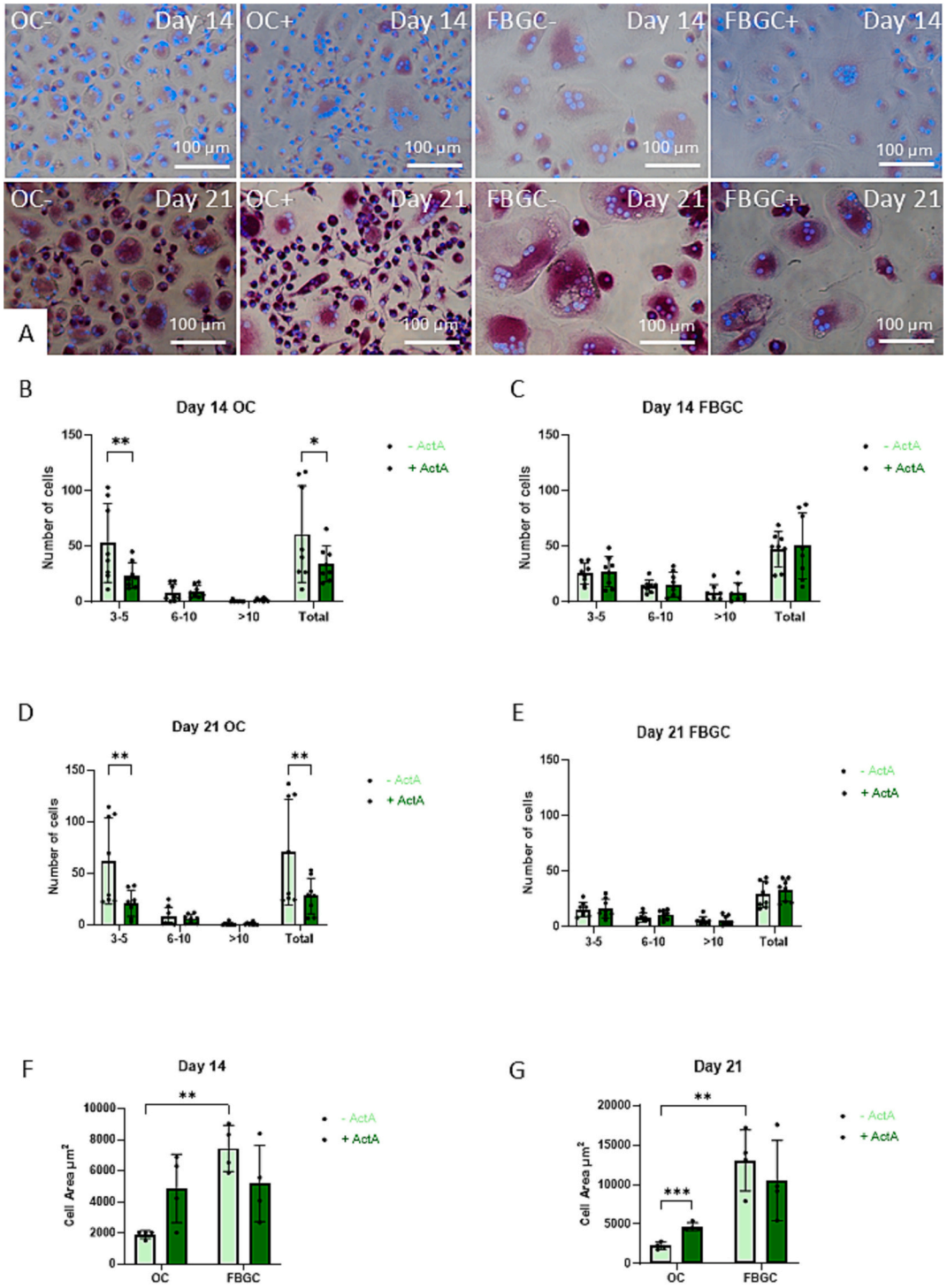

Fig. 1. ActA induces fewer but larger osteoclasts and does not have an effect on the number of FBGCs. A. Multinucleated TRAcP-positive cells differentiated from $CD14^+$ monocytes in osteoclast and FBGC cultures. Cells were cultured on plastic for 14 and 21 days with M-CSF and Rankl (osteoclasts) or M-CSF, IL-4, and IL-13 (FBGCs). Multinucleated cells were divided in 4 categories; cells with 3–5 nuclei (3–5), cells with 6 to 10 nuclei (6–10), cells with more than 10 nuclei (>10) or all multinucleated cells from category 1, 2 and 3 together (total). The intensity of the TRAcP-staining was stronger at 21 days of culture. B-E. ActA decreased the number of small multinucleated cells (3–5 nuclei) and the total number of multinucleated cells at both time points in osteoclast cultures (B&D). ActA did not affect the number of multinucleated cells in FBGC cultures (C&E). F & G. Multinucleated cells in FBGC cultures – ActA were larger compared to osteoclasts, but addition of ActA eliminated this difference (F&G). ActA increased the area of multinucleated osteoclasts significantly after 21 days (G). The cells were stained with DAPI to visualize nuclei (blue), and acid phosphatase leukocyte kit to visualize TRAcP (red). Images were taken with a 20× objective. $n = 8$ for cell counts, $n = 4$ for area measurement $^*p < 0.05$, $^{**}p < 0.01$. (For interpretation of the references to color in this figure legend, the reader is referred to the web version of this article.)

differences were not significant (Fig. 1 F). At both time points, in the control condition – ActA, the multinucleated cells were significantly larger in FBGC cultures compared to osteoclast cultures ($p < 0.01$), but not in the presence of ActA (Fig. 1 F and G). At day 21, ActA significantly increased the multinucleated cell area in osteoclast cultures ($p < 0.001$; Fig. 1 G).

3.3. The effect of ActA on cell morphology on bone is analogous to the observation on plastic

Multinucleated cells were observed in both osteoclast and FBGC cultures on bovine bone slices (Fig. 2 A). Analogous to cultures on plastic, the TRAcP staining was more intense after 21 days. We were not able to analyze the cell numbers on bone slices reliably due to the uneven background of the bone slice in light microscopy. However, the images show a trend for ActA in decreasing the number of small multinucleated cells in osteoclast cultures and inducing the formation of larger multinucleated cells. Thus, the effect of ActA seemed to be analogous to the effect on cultures on plastic. The images of FBGC cultures also seemed to show an effect similar to that on plastic, as ActA seemed not to have an effect on the cell number but decreased the area of the multinucleated cells. The confocal images from bone slices (Fig. 2 B) support these observations of decreased cell area in FBGC cultures.

3.4. ActA increases bone resorption by osteoclasts

Bone resorption was visualized with Field Emission Scanning Electron Microscopy (FESEM) and was observed only in osteoclast cultures (Fig. 3 A). 3D X-ray microscopy resorption pit analysis is shown in Fig. 3 B and presents the amount of bone resorption. ActA caused a significant increase in the resorptive activity of osteoclasts at day 21 (Fig. 3 C; $p < 0.01$). To account for slight warping and manufacturing imperfections in the bone slices, an overall 3D shape (baseplane) was detected and subtracted from the surface before area analysis. The imaging resolution was 2.79 μm per pixel. The increase in the amount of resorption after ActA treatment is evident. The FESEM images in Fig. 3 A confirm the presence of resorption pits on bone slices in osteoclast cultures. Resorption was not observed on bone slices after FBGC culture, however, the slices were occasionally covered with gray areas resembling cell remnants or slight etching of the cell surface. In confocal microscopy, similar structures were observed stained by phalloidin but lacking nuclei (data not shown), indicating the possibility of remnants of the actin cytoskeleton present on the bone surface.

3.5. ActA reduces the number of FBGCs on ALD

FESEM images show that multinucleated cells were present on ALD-HA surface in both osteoclast and FBGC cultures (Fig. 4 A). On ALD-HA ActA lost its effect of reducing the number of small multinucleated cells in osteoclast cultures (Fig. 4 B & D). In contrast, ActA significantly decreased the total number of multinucleated FBGCs on ALD-HA ($p < 0.05$; Fig. 4 C & E). Generally, on ALD-HA the osteoclast and FBGC cultures responded similarly, irrespective of the addition of ActA. We observed a slight trend of ActA reducing the number of multinucleated cells that formed in all groups and at all-time points, but the difference was not significant (Fig. 4 B–E). Fig. S2 represents the data of Fig. 4 in separate graphs for a detailed comparison between the groups based on the categorization of the cells by the number of nuclei (small multinucleated cells with 3–5 nuclei [Fig. S2 A & E], intermediate with 6–10 nuclei [Fig. S2 B & F] and large with >10 nuclei [Fig. S2 C & G]) and for comparison between the cell types. Considering the total number of multinucleated cells in the cultures without ActA, FBGCs had significantly more multinucleated cells at day 14 ($p < 0.05$; Fig. S2 D), but this difference was not present anymore at day 21 (Fig. S2 H).

Confocal microscopy images (Fig. 5) supported the observation that ActA does not have an effect on cell fusion on ALD-HA in osteoclast cultures but reduces the number of multinucleated cells in FBGC cultures. Multinucleated cells were observed in both cultures at both time points. In general, FBGCs seemed to be larger compared to osteoclasts, but we could not quantify the cell areas from confocal microscopy images. Further, both osteoclasts and FBGCs seemed to be larger on ALD-HA compared to bone (Fig. 2), but we were not able to quantify this difference reliably.

3.6. Acta influences gene expression differently in OC and FBGC

Linking all the above morphological data to more quantitative data at the cell level, qPCR was performed to assess gene expression of osteoclast and FBGC cultures on plastic, bone and ALD-HA. To further assess dynamics of gene expression, 3 weekly time points were assessed (7, 14 and 21 days). TRAcP, the osteoclast marker which is also expressed by FBGC's, showed a significant upregulation in osteoclast under the influence of ActA, but not in FBGC. TRAcP expression was lower in control FBGC cultures than in osteoclast cultures when ActA was added (Fig. 6A). These findings confirm our cell counting results since we observed a significantly lower number of FBGCs under control conditions. Also, the QPCR analysis confirmed our previous findings on the effect of ActA on osteoclasts; the expression of 3 genes we previously found to be highly upregulated during the ActA induced formation of giant osteoclasts, namely master regulator of MHC class II (CIITA), oxidized low-density lipoprotein receptor 1 (OLR1) and Rho-related BTB domain-containing protein 1 (RHOBTB1), was again upregulated in the osteoclast cultures under the influence of ActA [45]. In contrast, ActA did not result in a changed expression of these genes in FBGC cultures (Fig. 6B, C and D). Gene expression of the canonical ActA receptor ALK4 was significantly lower in FBGCs compared to osteoclasts (Fig. 6 E), which could explain the lack of effect of ActA on the FBGCs. Interestingly, TRAcP, CIITA and RHOBTB1 were not upregulated in osteoclast cultures with ActA on bone or ALD (Fig. 7 A, B & D). The expression of CIITA and OLR1 was significantly higher when cells were cultured on bone compared to plastic or ALD (Fig. 7 B & C). ALK4 expression was significantly higher on bone compared to plastic, but no difference in expression of this gene was found between cultures on bone and ALD (Fig. 7E, C). The qPCR results of DC-STAMP (fusion molecule expressed in osteoclasts and FBGCs) (Fig. 6F and Fig. 7F) and Tcirg (V-ATPase [ATP-driven proton pump active in extracellular acidification during resorption] subunit, data not shown) showed no differences between osteoclasts and FBGCs, and ActA did not have a clear effect on the expression of these genes.

4. Discussion

With the gradual growth of knowledge on the diverse types of multinucleated cells, their functions and the way they form, we are on the verge of entering a new era where we can specifically interfere with certain multinucleated cells, while leaving the other untouched. Activin A represents one such potential regulator. Here, we unequivocally show that ActA has a different effect on osteoclasts compared to FBGCs.

ActA has been shown to have either stimulatory [23,25–29,32] or inhibitory [31] effects on osteoclastogenesis. We have previously shown that ActA decreases osteoclastogenesis but increases the size of osteoclasts differentiated from human $CD14^+$ monocytes [43,44]. This study confirmed the earlier results, as in osteoclast cultures we observed decreased osteoclastogenesis of small osteoclasts. Further, as in our previous study, ActA increased the number of large multinucleated cells with >10 nuclei, which was confirmed by the area analysis of the cells. The multinucleated cells in osteoclast cultures with ActA were larger compared to cultures without ActA (Fig. 2), which explains the reduced number of small multinucleated cells upon the addition of ActA, as the cells fused into giant multinucleated cells in response to ActA. Also, these larger osteoclasts were more active as shown by their enhanced resorption.

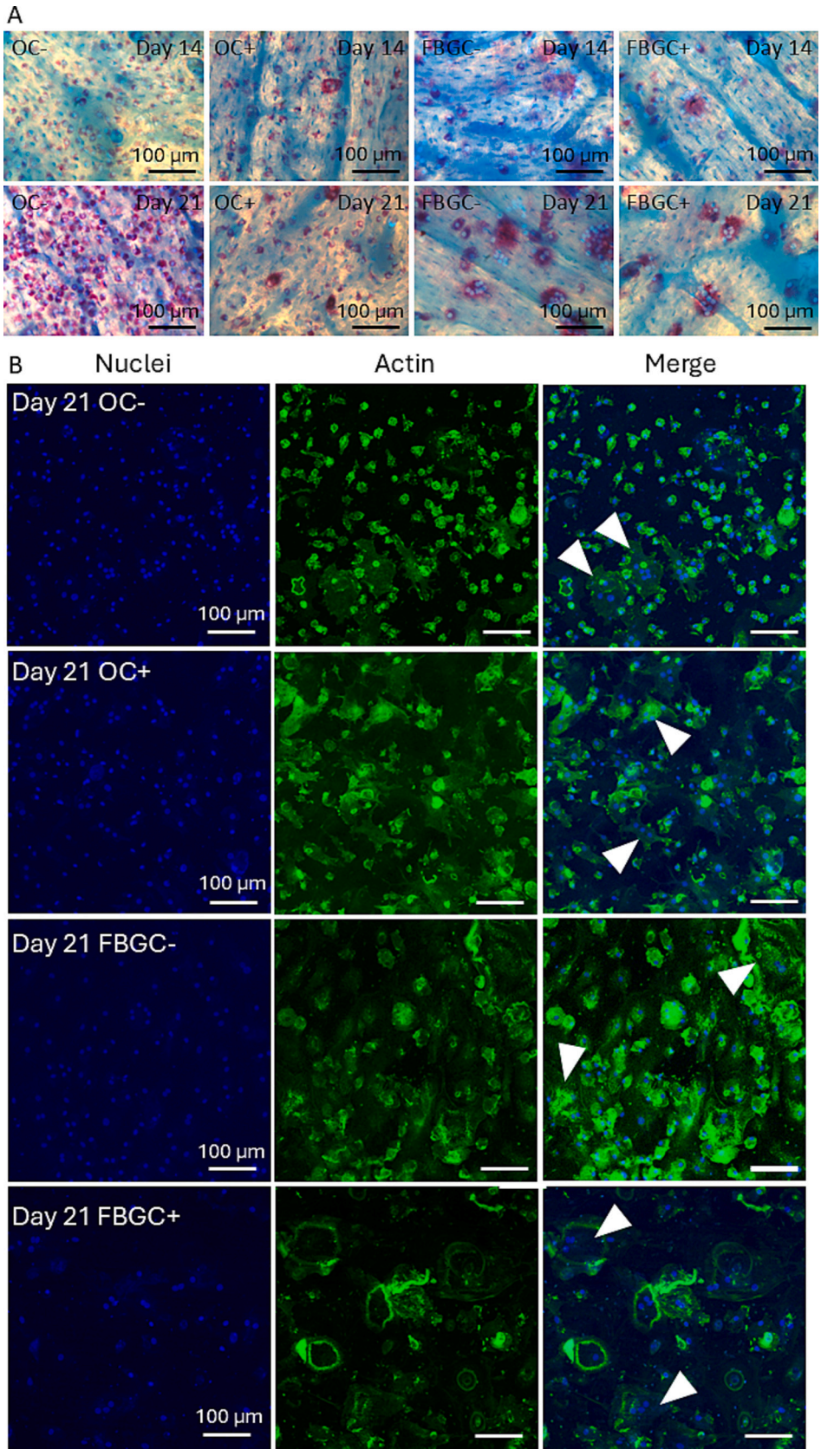

(caption on next page)

Fig. 2. The morphology of osteoclasts and FBGCs on bovine bone slices. A. Multinucleated TRAcP-positive cells differentiated from $CD14^+$ monocytes in osteoclast and FBGC cultures on bone. Cells were cultured on bovine bone slices for 14 and 21 days with M-CSF and Rankl (osteoclasts) or M-CSF, IL-4, and IL-13 (FBGCs). The intensity of the TRAcP-staining was stronger at 21 days of culture. The effect of ActA on cell fusion was similar to the effect on plastic, as ActA seemed to decrease the number of small osteoclasts, induce the formation of large osteoclasts, but had no effect on the number of FBGCs. Instead, ActA decreased the area of FBGCs. B. Confocal microscopy images support the observations from the light microscopy images. Multinucleated cells are marked with arrowheads. The actin cytoskeleton was stained with Alexa 488-conjugated phalloidin (green) and nuclei were stained with Hoechst (blue). Both light and confocal microscopy images were taken with a 20× objective. (For interpretation of the references to color in this figure legend, the reader is referred to the web version of this article.)

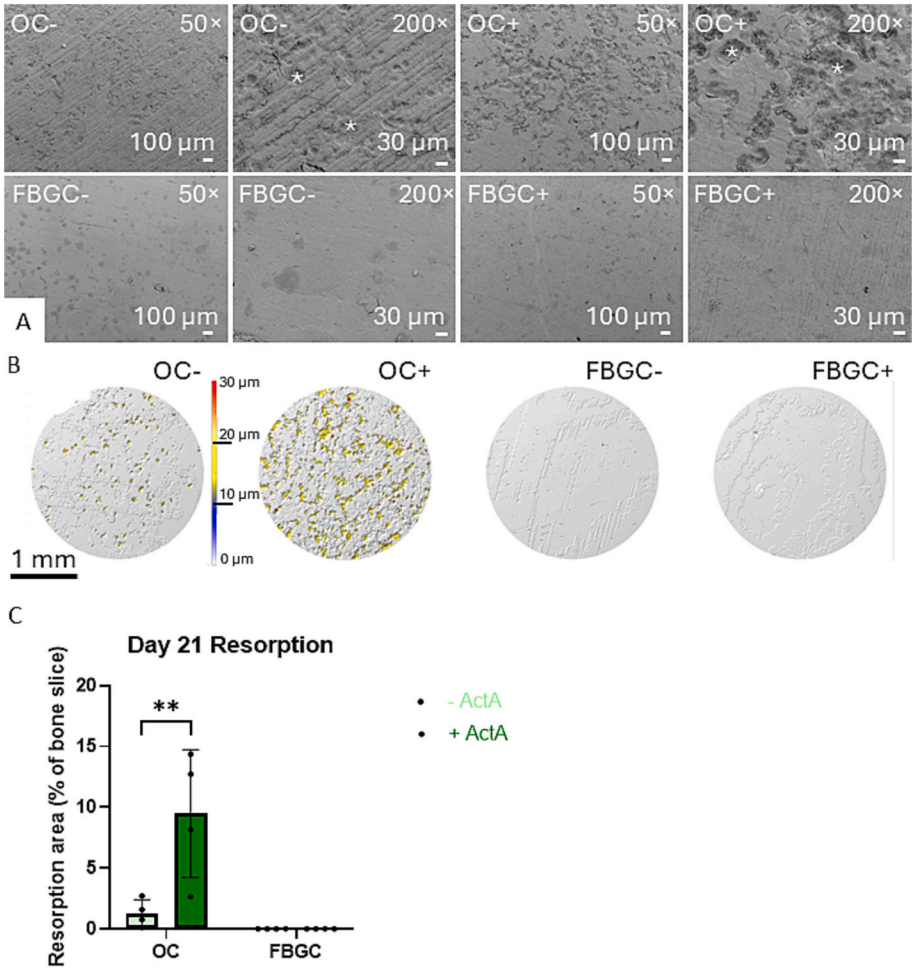

Fig. 3. ActA increases bone resorption by osteoclasts. A. FESEM images of bone slices show resorption pits in osteoclast samples. ActA increased resorption by osteoclasts. No resorption was observed by FBGCs, and ActA did not have an effect on FBGCs concerning resorption. B. Demonstrative images for resorption pit analysis by 3D X-ray microscopy show increased resorption by osteoclasts after ActA treatment, but no resorption by FBGCs. C. 3D X-ray microscopy analysis of the resorption pit area confirmed the observation that ActA increases resorption by osteoclasts ($p < 0.01$). Resorption pits in A are marked with an asterisk. In B, the depth of the pits is demonstrated with a color bar next to the image of the bone slice. n = 4, $^{**}p < 0.01$.

A contrary result was observed in FBGC cultures, since ActA did not increase the FBGC area. We conclude that ActA has a different effect on osteoclasts and FBGCs regarding cell fusion.

Under normal circumstances, ActA signals via the ALK4 or ALK7 type I BMP receptors. Our qPCR results show a significantly lower ALK4 expression in FBGCs compared to osteoclasts (ALK7 was not expressed in any of the experimental conditions, data not shown). This could be an explanation for the observed results where ActA influenced osteoclast fusion and resorptive activity and induced differential gene expression, whereas it did not have this effect on FBGCs. In our previous study, we showed that ActA induced the formation of large osteoclasts, and RNAseq data showed that especially CIITA, ORL1 and RHOBTB1 were highly upregulated in these cultures that contained giant osteoclasts. Since FBGCs are generally larger than osteoclasts, we assumed that these genes would also be more highly expressed in FBGC cultures (regardless of the addition of ActA) compared to normal osteoclast cultures. Our qPCR data shows that this is not the case, suggesting that the fusion mechanism underlying the formation of the large osteoclast under the influence of ActA could be subtly different from the fusion mechanism that gives rise to the big FBGCs. Further, the fusion mechanism on the different substrates seemed to alternate, as on bone and ALD-HA the upregulation of TRAcP, CIITA and RHOBTB1 in osteoclast cultures with ActA was not present or less striking. Interestingly, fueling the idea that fusion is context dependent, the expression of CIITA, OLR1 and ALK4 was higher when osteoclasts were cultured on bone compared to plastic or ALD. We have previously shown that the surface roughness of the bone slices and ALD-HA samples is different [60], offering one explanation for the results, as surface topography acts as a guide for the cell differentiation [61,62]. Alternatively, bone is rich in extracellular matrix proteins that are known activators of osteoclast formation [63].

Osteoclasts are known to be activated by proinflammatory signals [64,65], and ActA is one of the proteins having either anti- or

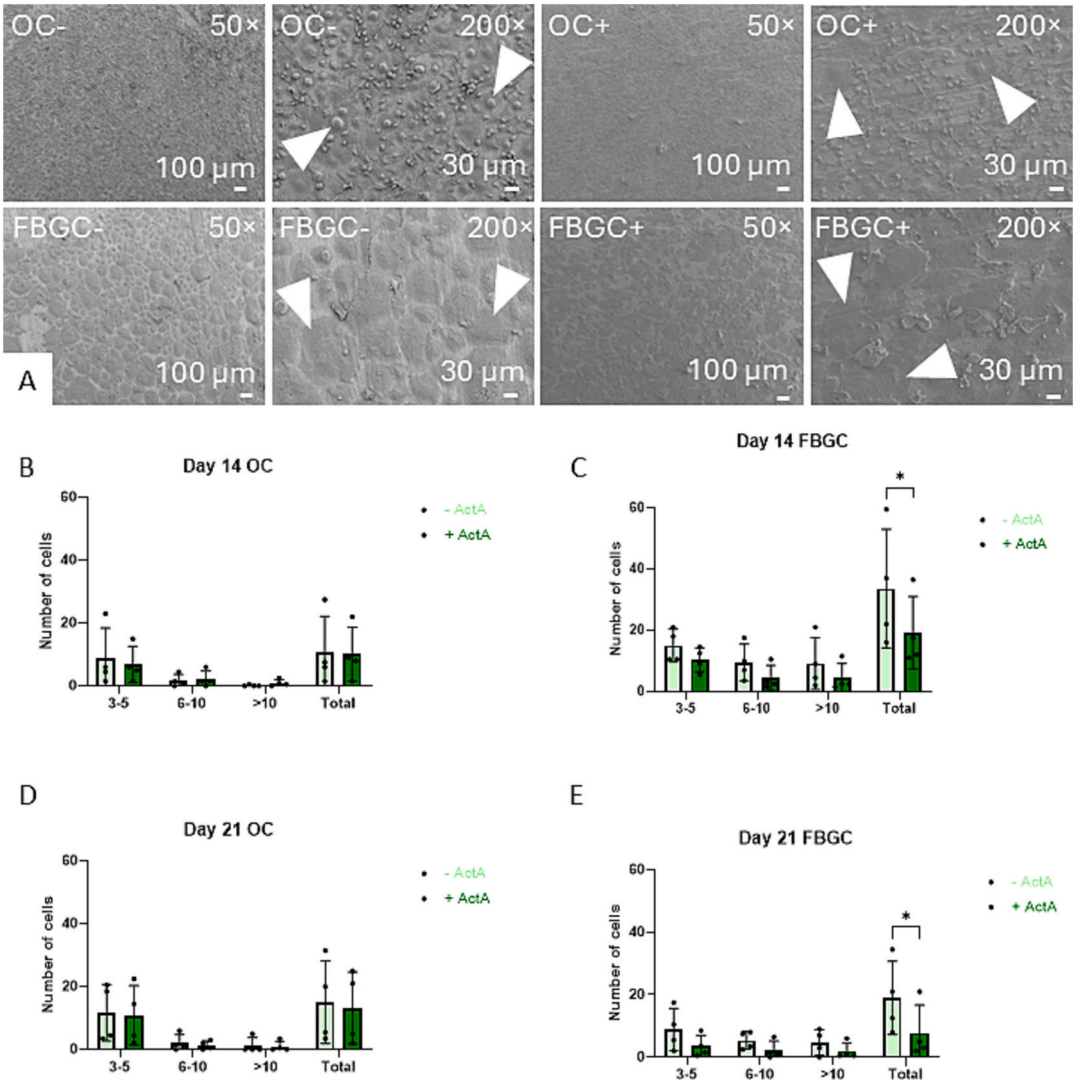

Fig. 4. ActA reduces the number of FBGCs on ALD-HA. A. FESEM images show multinucleated cells on ALD-HA surface in both osteoclast and FBGC cultures. The morphology of osteoclasts was dome-like with a surrounding flat area, whereas FBGCs presented as large, low and flat cells. ActA did not have an effect on multinucleated cell number in osteoclast cultures (B & D) but decreased the total number of multinucleated cells in FBGC cultures on ALD-HA (C & E), as assessed by confocal microscopy. n = 4, $*p < 0.05$.

proinflammatory effects in tissues [36–39,41,42]. It is possible that in osteoclast cultures ActA acts as a proinflammatory agent causing the formation of so-called pathological osteoclasts with enhanced bone resorption properties [66]. These osteoclasts form in response to excess inflammation and are harmful regarding the long-term survival of bone implants, as the overactive osteoclasts cause excess peri-implant bone resorption leading to implant loosening [67–70]. Our results might suggest a contrary, anti-inflammatory effect of ActA in FBGC cultures. FBGCs are already large cells (with an inflammatory function), that are formed without any influence of ActA. It's possible that they do not need further activation through the ActA receptor, instead, the signaling via the receptor drives the attenuation of the inflammatory reaction, leading to decreased FBGC area and number, which could be beneficial for implant integration.

In our previous study with human peripheral blood monocytes (PBMC) from healthy donors [60] we observed normal osteoclastogenesis on bone, but on hydroxyapatite-coated titanium (ALD-HA), large FBGC-resembling cells were formed. We studied osteoclastogenesis and FBGC differentiation on the same biomaterials in this study, but now using the $CD14^+$ monocytes isolated from the PBMC as precursor cells. As in our previous study, the $CD14^+$ monocytes differentiated into larger multinucleated cells on ALD-HA compared to bone. We were not able to measure the cell areas on ALD-HA, since the non-transparent Ti samples require confocal microscopy for viewing the cells, and it was not possible to do a quantitative analysis with it due to laborious imaging methods. However, the confocal microscopy images demonstrate a different cell morphology on ALD-HA samples compared to bone, which suggests an alternative differentiation process on this surface. In our previous study, we suggested that the cells on ALD-HA could be FBGCs instead of osteoclasts and that the surface topography might be one of the causes of this difference. Here, on the other hand, when using the cytokines that steer differentiation of osteoclasts (M-CSF and RANKL) and FBGCs (M-CSF and IL-4 and IL-13), culture on ALD-HA resulted in distinctively different morphologies, where addition of ActA did not influence these morphologies. Bone surface roughness was shown to be greater compared to ALD-HA [60], and osteoclastogenesis is found to be favored on a rough surface [12,61,62,71–73]. A similar mechanism of increased FBGC differentiation on smoother ALD-HA might be behind the results of this study.

In this study, we also differentiated FBGCs from $CD14^+$ monocytes with IL-4 and IL-13. As osteoclasts, FBGCs on ALD-HA were considerably larger on ALD-HA than on bone, supporting the idea that ALD-HA

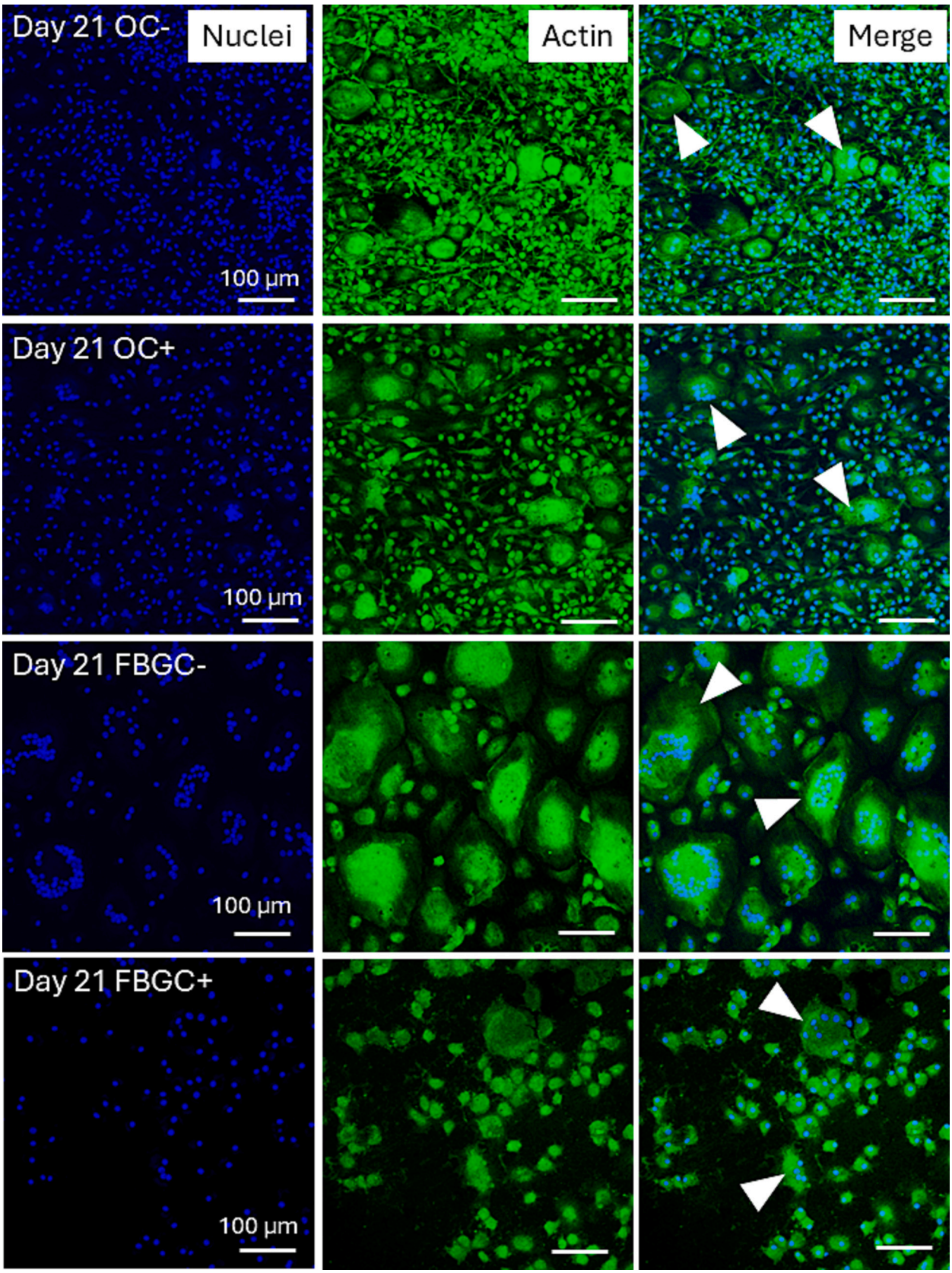

Fig. 5. The morphology of osteoclasts and FBGCs on ALD-HA. Confocal microscopy images of ALD-HA support the observation of ActA not having an effect on osteoclast number but reducing the multinucleated FBGC number. Multinucleated osteoclasts and FBGCs (arrowheads) were observed on ALD-HA, with and without ActA. The actin cytoskeleton was stained with Alexa 488-conjugated phalloidin (green) and nuclei were stained with Hoechst (blue). Images were taken with a 20× objective. (For interpretation of the references to color in this figure legend, the reader is referred to the web version of this article.)

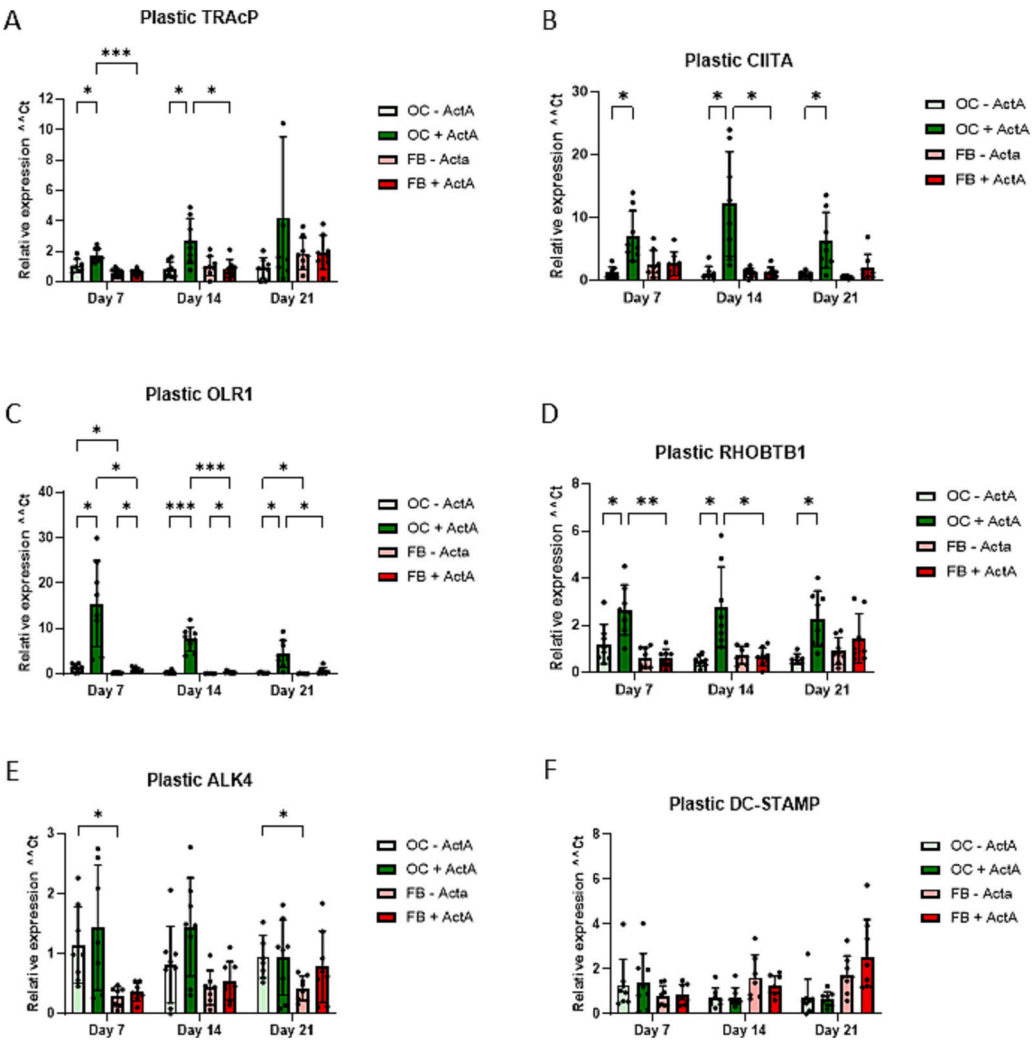

Fig. 6. mRNA expression in osteoclast and FBGC cultures on plastic. A. TRAcP was upregulated in osteoclasts, but not in FBGCs after stimulation with ActA. TRAcP was expressed at lower levels in FBGCs compared to osteoclasts. B–D. ActA induced the upregulation of CIITA, OLR1 and RHOBTB1 in osteoclasts but not in FBGCs. E. The canonical ActA receptor ALK4 was significantly lower in FBGCs compared to osteoclasts. F. Expression of DC-STAMP did not change over time and is the same in OC and FBGC. Responses of FBGC were inert in terms of time points (7, 14, 21 days) or condition (without or with ActA). n = 8, $*p < 0.05$. $**p < 0.01$ $***p < 0.001$.

surface causes a foreign body reaction by the stimulation of large FBGC formation. An interesting observation considering the number of multinucleated cells upon treatment with ActA is that on ALD-HA, ActA did not have an effect on osteoclast number. Thus, ActA seemed to lose the effect of reducing the number of small osteoclasts and increasing the cell fusion into larger multinucleated cells. In fact, osteoclasts on ALD-HA started to resemble FBGCs in this regard, which supports our hypothesis of the ALD-HA as a foreign body reaction-inducing material. The response of the IL-differentiated FBGCs to ActA on ALD-HA was consistent regarding small, intermediate and giant FBGCs, as ActA decreased the number of these cells at both time points, albeit not significantly. Thus, on ALD-HA, ActA downregulated the differentiation of these cells, but the mechanism behind this remains elusive. Possible explanations are the differences in the release of ions from the materials, pH, and a differing cytokine expression from the cells upon attachment to these materials [74].

Taken together, our results show that ActA induces fewer, but larger and more active osteoclasts both on plastic as well as on their natural substrate bone. This effect is not present in FBGC, possibly due to the significantly lower expression of the canonical ActA receptor ALK4. On ALD-HA this influence of ActA on osteoclasts is not present anymore, instead, the osteoclasts seem to be larger and lose their response to ActA on this biomaterial.

CRediT authorship contribution statement

Elina Kylmäoja: Writing – review & editing, Writing – original draft, Visualization, Validation, Project administration, Methodology, Investigation, Formal analysis, Data curation, Conceptualization. **Sami Kauppinen:** Writing – review & editing, Writing – original draft, Visualization, Validation, Software, Resources, Methodology, Investigation, Formal analysis, Data curation. **Faleh Abushahba:** Writing – review & editing, Resources. **Mikko Finnilä:** Writing – review & editing, Validation, Supervision, Software, Resources, Methodology, Funding acquisition. **Mikko Ritala:** Writing – review & editing, Resources, Methodology. **Petri Lehenkari:** Writing – review & editing, Supervision. **Juha Tuukkanen:** Writing – review & editing, Supervision. **Teun J. de Vries:** Writing – review & editing, Validation, Supervision, Methodology, Conceptualization. **Ton Schoenmaker:** Writing – review & editing, Writing – original draft, Visualization, Validation, Supervision, Resources, Project administration, Methodology, Investigation, Formal analysis, Data curation, Conceptualization.

Declaration of Generative AI and AI-assisted technologies in the writing process

During the preparation of this work the authors used ChatGPT to

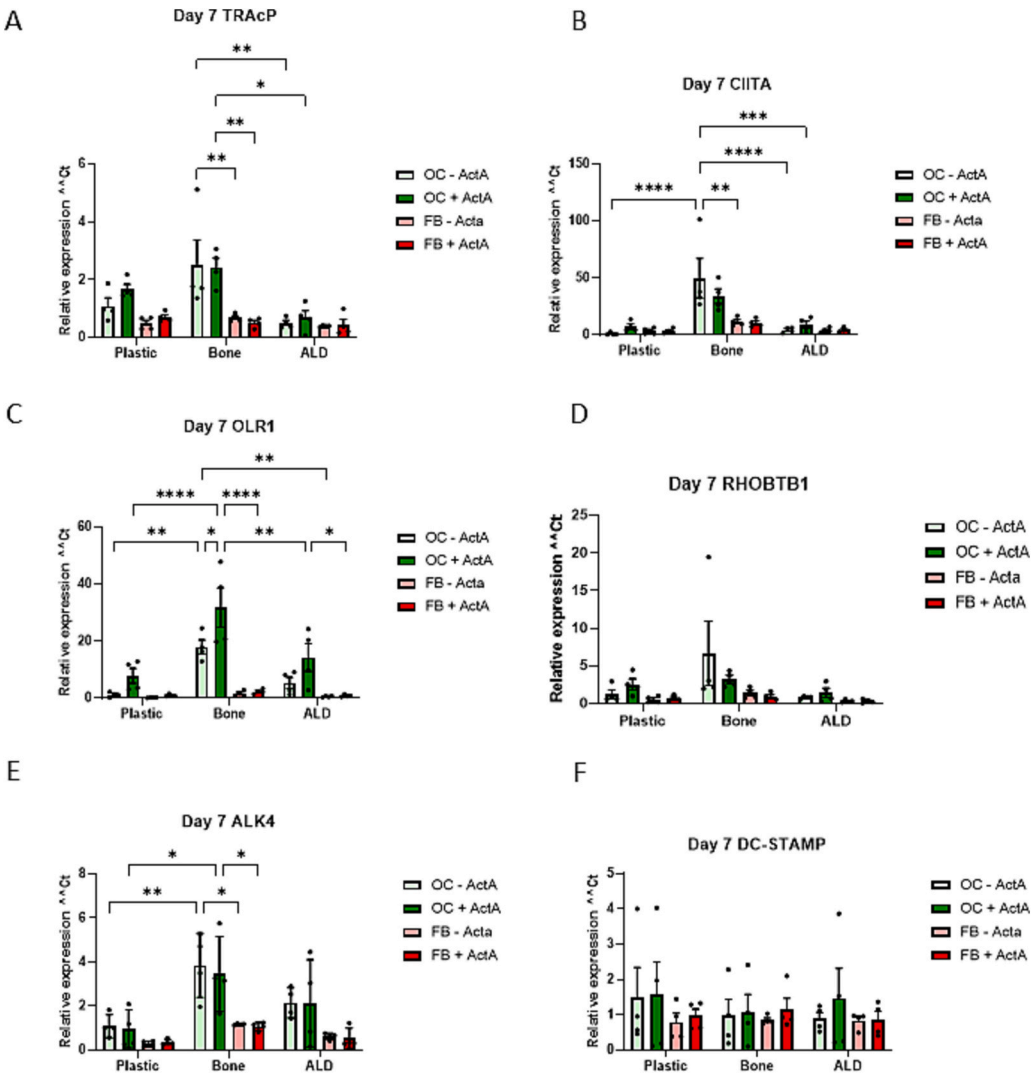

Fig. 7. mRNA expression in osteoclast and FBGC cultures on plastic, bone and ALD. A, B & D. On bone and ALD, the upregulation of TRAcP, CIITA and RHOBTB1 in osteoclast cultures with ActA disappeared. B, C & E. The expression of CIITA, OLR1 and ALK4 was significantly higher when cells were cultured on bone compared to plastic or ALD. F. There was no statistical difference in DC-STAMP expression between the different substrates. Responses of FBGC were inert in terms of time points (7, 14, 21 days) or condition (without or with ActA). n = 4, *$p < 0.05$. **p < 0.01 ***p < 0.001 ****$p < 0.0001$.

improve the readability and language of the manuscript. After using this tool, the authors reviewed and edited the content as needed and take full responsibility for the content of the published article.

Funding sources

This project is supported by Research Council of Finland (project number 347445, 353755) and Jane and Aatos Erkko Foundation to support X-ray microscopy and related analysis.

Declaration of competing interest

The authors declare that they have no known competing financial interests or personal relationships that could have appeared to influence the work reported in this paper.

Acknowledgements

Biocenter Oulu Light Microscopy Core Facility and Biocenter Oulu Electron Microscopy Core Facility, University of Oulu, supported by Biocenter, Finland, are acknowledged for their assistance with confocal and electron microscopic analysis. Dr. Jani Holopainen is greatly acknowledged for making the HA coatings.

Appendix A. Supplementary data

Supplementary data to this article can be found online at https://doi.org/10.1016/j.bone.2026.117814.

Data availability

Data will be made available on request.

References

[1] K. Ahmadzadeh, M. Vanoppen, C.D. Rose, P. Matthys, C.H. Wouters, Multinucleated giant cells: current insights in phenotype, biological activities, and mechanism of formation, Front. Cell Dev. Biol. 10 (2022).
[2] M. Yagi, et al., DC-STAMP is essential for cell–cell fusion in osteoclasts and foreign body giant cells, J. Exp. Med. 202 (2005) 345–351.
[3] B. Ten Harkel, et al., The foreign body giant cell cannot resorb bone, but dissolves hydroxyapatite like osteoclasts, PloS One 10 (2015).
[4] U.A. Khan, S.M. Hashimi, M.M. Bakr, M.R. Forwood, N.A. Morrison, Foreign body giant cells and osteoclasts are TRAP positive, have podosome-belts and both require OC-STAMP for cell fusion, J. Cell. Biochem. 114 (2013) 1772–1778.

[5] R.J. Miron, H. Zohdi, M. Fujioka-Kobayashi, D.D. Bosshardt, Giant cells around bone biomaterials: osteoclasts or multi-nucleated giant cells? Acta Biomater. 46 (2016) 15–28.
[6] M. Pereira, et al., Common signalling pathways in macrophage and osteoclast multinucleation, J. Cell Sci. 131 (2018).
[7] K. Ahmadzadeh, et al., Multinucleation resets human macrophages for specialized functions at the expense of their identity, EMBO Rep. 24 (2023).
[8] J. Halper, B. Dolfi, S. Ivanov, M.B. Madel, C. Blin-Wakkach, Macrophages and osteoclasts: similarity and divergence between bone phagocytes, Front. Immunol. 16 (2025) 1683872.
[9] L.J. Raggatt, N.C. Partridge, Cellular and Molecular Mechanisms of Bone Remodeling * Cells Involved in Bone Remodeling, 2010, https://doi.org/10.1074/jbc.R109.041087.
[10] S. Bolamperti, I. Villa, A. Rubinacci, Bone remodeling: an operational process ensuring survival and bone mechanical competence, Bone Res. 10 (2022) 1–19, 2022 10:1.
[11] Z. Sheikh, et al., Macrophages, foreign body giant cells and their response to implantable biomaterials, Materials 8 (2015) 5671–5701.
[12] N.L. Davison, et al., Osteoclast resorption of beta-tricalcium phosphate controlled by surface architecture, Biomaterials 35 (2014) 7441–7451.
[13] M. Haga, et al., Detailed process of bone remodeling after achievement of osseointegration in a rat implantation model, Anat. Rec. 292 (2009) 38–47.
[14] A. Insua, A. Monje, H.-L. Wang, R.J. Miron, Basis of Bone Metabolism Around Dental Implants During Osseointegration and Peri-implant Bone Loss, 2017, https://doi.org/10.1002/jbm.a.36060.
[15] A. Mavrogenis, R. Dimitriou, J. Parvizi, G. Babis, Biology of implant osseointegration, J. Musculoskelet. Neuronal Interact. 9 (2009) 61–71.
[16] R. Trindade, T. Albrektsson, P. Tengvall, A. Wennerberg, Foreign Body Reaction to Biomaterials: On Mechanisms for Buildup and Breakdown of Osseointegration, 2014, https://doi.org/10.1111/cid.12274.
[17] Y. Chandorkar, K. Ravikumar, B. Basu, The foreign body response demystified, ACS Biomater Sci. Eng. 5 (2019) 19–44.
[18] F. Eslami-Kaliji, N. Hedayat Nia, J.R.T. Lakey, A.M. Smink, M. Mohammadi, Mechanisms of foreign body giant cell formation in response to implantable biomaterials, Polymers 15 (2023). Preprint at https://doi.org/10.3390/polym15051313.
[19] E. Gibon, et al., Friend or foe? Inflammation and the foreign body response to orthopedic biomaterials, J. Biomed. Mater. Res. 112 (2024) 1172–1187.
[20] E. Bloise, et al., Activin A in mammalian physiology, Physiol. Rev. 99 (2019) 739–780.
[21] M. Centrella, T.L. Mccarthy, E. Canalis, Activin-A binding and biochemical effects in osteoblast-enriched cultures from fetal-rat parietal bone, Mol. Cell. Biol. 11 (1991) 250.
[22] M. Eijken, et al., The activin A-follistatin system: potent regulator of human extracellular matrix mineralization, FASEB J. 21 (2007) 2949–2960.
[23] D. Gaddy-Kurten, J.K. Coker, E. Abe, R.L. Jilka, S.C. Manolagas, Inhibin suppresses and activin stimulates osteoblastogenesis and osteoclastogenesis in murine bone marrow cultures, Endocrinology 143 (2002) 74–83.
[24] R.D.A.M. Alves, M. Eijken, K. Bezstarosti, J.A.A. Demmers, J.P.T.M. Van Leeuwen, Activin A suppresses osteoblast mineralization capacity by altering extracellular matrix (ECM) composition and impairing matrix vesicle (MV) production, Mol. Cell. Proteomics 12 (2013) 2890–2900.
[25] K. Fuller, K.E. Bayley, T.J. Chambers, Activin A is an essential cofactor for osteoclast induction, Biochem. Biophys. Res. Commun. 268 (2000) 2–7.
[26] R. Sakai, Y. Eto, M. Ohtsuka, M. Hirafuji, H. Shinoda, Activin enhances osteoclast-like cell formation in vitro, Biochem. Biophys. Res. Commun. 195 (1993) 39–46.
[27] T. Sugatani, U.M. Alvarez, K.A. Hruska, Activin A stimulates IkappaB-alpha/NFkappaB and RANK expression for osteoclast differentiation, but not AKT survival pathway in osteoclast precursors, J. Cell. Biochem. 90 (2003) 59–67.
[28] T. Kajita, et al., Mechanisms involved in enhancement of osteoclast formation by activin-A, J. Cell. Biochem. 119 (2018) 6974–6985.
[29] M. Omi, V. Kaartinen, Y. Mishina, Activin A receptor type 1-mediated BMP signaling regulates RANKL-induced osteoclastogenesis via canonical SMAD-signaling pathway, J. Biol. Chem. 294 (2019) 17818–17836.
[30] Y. Ogawa, et al., Bovine bone activin enhances bone morphogenetic protein-induced ectopic bone formation, J. Biol. Chem. 267 (1992) 14233–14237.
[31] T.W. Fowler, et al., Activin A inhibits RANKL-mediated osteoclast formation, movement and function in murine bone marrow macrophage cultures, J. Cell Sci. 128 (2015) 683–694.
[32] T. Koseki, et al., Role of TGF-β family in osteoclastogenesis induced by RANKL, Cell. Signal. 14 (2002) 31–36.
[33] R.S. Pearsall, et al., A soluble activin Type IIA receptor induces bone formation and improves skeletal integrity, Proc. Natl. Acad. Sci. U. S. A. 105 (2008) 7082–7087.
[34] K.L. Jones, et al., Activin A is a critical component of the inflammatory response, and its binding protein, follistatin, reduces mortality in endotoxemia, Proc. Natl. Acad. Sci. U. S. A. 104 (2007) 16239–16244.
[35] K.L. Jones, J.N. Brauman, N.P. Groome, D.M. De Kretser, D.J. Phillips, Activin A release into the circulation is an early event in systemic inflammation and precedes the release of follistatin, Endocrinology 141 (2000) 1905–1908.
[36] R.M. Nüsing, J. Barsig, Induction of prostanoid, nitric oxide, and cytokine formation in rat bone marrow derived macrophages by activin A, Br. J. Pharmacol. 127 (1999) 919–926.
[37] R.M. Nüsing, S. Mohr, V. Ullrich, Activin A and retinoic acid synergize in cyclooxygenase-1 and thromboxane synthase induction during differentiation of J774.1 macrophages, Eur. J. Biochem. 227 (1995) 130–136.
[38] M. Abe, et al., Potent induction of activin A secretion from monocytes and bone marrow stromal fibroblasts by cognate interaction with activated T cells, J. Leukoc. Biol. 72 (2002) 347–352.
[39] D.M. de Kretser, R.E. O'Hehir, C.L. Hardy, M.P. Hedger, The roles of activin A and its binding protein, follistatin, in inflammation and tissue repair, Mol. Cell. Endocrinol. 359 (2012) 101–106. Preprint at https://doi.org/10.1016/j.mce.2011.10.009.
[40] I. Morianos, G. Papadopoulou, M. Semitekolou, G. Xanthou, Activin-A in the regulation of immunity in health and disease, J. Autoimmun. 104 (2019). Preprint at https://doi.org/10.1016/j.jaut.2019.102314.
[41] F. Li, Y. Long, X. Yu, Y. Tong, L. Gong, Different immunoregulation roles of activin A compared with TGF-β, Front. Immunol. 13 (2022). Preprint at https://doi.org/10.3389/fimmu.2022.921366.
[42] E. Sierra-Filardi, et al., Activin A Skews Macrophage Polarization by Promoting a Proinflammatory Phenotype and Inhibiting the Acquisition of Anti-inflammatory Macrophage Markers, 2011, https://doi.org/10.1182/blood-2010.
[43] T. Schoenmaker, et al., The effect of Activin-A on periodontal ligament fibroblasts-mediated osteoclast formation in healthy donors and in patients with fibrodysplasia ossificans progressiva, J. Cell. Physiol. 234 (2019) 10238–10247.
[44] T. Schoenmaker, et al., Activin-A induces fewer, but larger osteoclasts from monocytes in both healthy controls and Fibrodysplasia Ossificans Progressiva patients, Front. Endocrinol. (Lausanne) 11 (2020) 501.
[45] T. Schoenmaker, et al., Transcriptomic differences underlying the activin-A induced large osteoclast formation in both healthy control and fibrodysplasia ossificans progressiva osteoclasts, Int. J. Mol. Sci. 24 (2023).
[46] C. Pabinger, H. Lothaller, N. Portner, A. Geissler, Projections of hip arthroplasty in OECD countries up to 2050, Hip Int. 28 (2018) 498–506.
[47] E. Kylmäoja, J. Holopainen, F. Abushahba, M. Ritala, J. Tuukkanen, Osteoblast attachment on titanium coated with hydroxyapatite by atomic layer deposition, Biomolecules 12 (2022).
[48] N. Areid, et al., Impact of atomic layer-deposited hydroxyapatite-coated titanium on expression of focal adhesion molecules of human gingival fibroblasts, Nanomaterials 15 (2025) 887, 2025, Vol. 15, Page 887.
[49] F. Abushahba, et al., Gingival keratinocyte adhesion on atomic layer-deposited hydroxyapatite coated titanium, J. Biomater. Appl. 39 (2025).
[50] S. Hashemi Astaneh, L.P. Faverani, C. Sukotjo, C.G. Takoudis, Atomic layer deposition on dental materials: processing conditions and surface functionalization to improve physical, chemical, and clinical properties - a review, Acta Biomater. 121 (2021) 103–118. Preprint at https://doi.org/10.1016/j.actbio.2020.11.024.
[51] P.O. Oviroh, R. Akbarzadeh, D. Pan, R.A.M. Coetzee, T.C. Jen, New development of atomic layer deposition: processes, methods and applications, Sci. Technol. Adv. Mater. 20 (2019) 465–496. Preprint at https://doi.org/10.1080/14686996.2019.1599694.
[52] S. Bose, S. Tarafder, A. Bandyopadhyay, Hydroxyapatite coatings for metallic implants, in: Hydroxyapatite (Hap) for Biomedical Applications, Woodhead Publishing, Cambridge, UK, 2015, pp. 143–157, https://doi.org/10.1016/b978-1-78242-033-0.00007-9.
[53] J. Faig-Martí, F.J. Gil-Mur, Hydroxyapatite coatings in prosthetic joints, Revista Española de Cirugía Ortopédica y Traumatología (English Edition) 52 (2008) 113–120.
[54] L. Sun, C.C. Berndt, K.A. Gross, A. Kucuk, Material fundamentals and clinical performance of plasma-sprayed hydroxyapatite coatings: a review, J. Biomed. Mater. Res. 58 (2001) 570–592.
[55] J. Holopainen, et al., Preparation and bioactive properties of nanocrystalline hydroxyapatite thin films obtained by conversion of atomic layer deposited calcium carbonate, Biointerphases 9 (2014) 031008.
[56] O. Nilsen, H. Fjellvåg, A. Kjekshus, Growth of calcium carbonate by the atomic layer chemical vapour deposition technique, Thin Solid Films 450 (2004) 240–247.
[57] P. Bankhead, et al., QuPath: Open source software for digital pathology image analysis, Sci. Rep. 7 (2017) 1–7, 2017 7:1.
[58] N. Otsu, Threshold selection method from gray-level histograms, IEEE Trans. Syst. Man Cybern. SMC-9 (1979) 62–66.
[59] J. D'Errico, Surface Fitting using gridfit. https://www.mathworks.com/matlabcentral/fileexchange/8998-surface-fitting-using-gridfit, 2008.
[60] E. Kylmäoja, F. Abushahba, J. Holopainen, M. Ritala, J. Tuukkanen, Monocyte differentiation on atomic layer-deposited (ALD) hydroxyapatite coating on titanium substrate, Molecules 28 (2023) 3611, 2023, Vol. 28, Page 3611.
[61] M. Nagasawa, et al., Topography influences adherent cell regulation of osteoclastogenesis, J. Dent. Res. 95 (2016) 319–326.
[62] B. Sommer, et al., Wear particles and surface topographies are modulators of osteoclastogenesis in vitro, J. Biomed. Mater. Res. A 72 (2005) 67–76.
[63] Z. Yao, L. Xing, C. Qin, E.M. Schwarz, B.F. Boyce, Osteoclast precursor interaction with bone matrix induces osteoclast formation directly by an interleukin-1-mediated autocrine mechanism, J. Biol. Chem. 283 (2008) 9917–9924.
[64] J. Zupan, M. Jeras, J. Marc, Osteoimmunology and the influence of pro-inflammatory cytokines on osteoclasts, Biochem. Med. (Zagreb.) 23 (2013) 43–63.
[65] L. Xing, E.M. Schwarz, B.F. Boyce, Osteoclast precursors, RANKL/RANK, and immunology, Immunol. Rev. 208 (2005) 19–29.
[66] M.B. Madel, et al., Immune function and diversity of osteoclasts in normal and pathological conditions, Front. Immunol. 10 (2019) 1408.
[67] D.R. Haynes, T.N. Crotti, H. Zreiqat, Regulation of osteoclast activity in peri-implant tissues, Biomaterials 25 (2004) 4877–4885. Preprint at https://doi.org/10.1016/j.biomaterials.2004.01.003.
[68] S. Sprangers, T. Schoenmaker, Y. Cao, V. Everts, T.J. de Vries, Different blood-borne human osteoclast precursors respond in distinct ways to IL-17A, J. Cell. Physiol. 231 (2016) 1249–1260.

[69] Y. Meirow, et al., Specific Inflammatory Osteoclast Precursors Induced During Chronic Inflammation Give Rise to Highly Active Osteoclasts Associated With Inflammatory Bone Loss, Bone Res. 10 (1) (2022) 36, https://doi.org/10.1038/s41413-022-00206-z.
[70] Y. Meirow, et al., Specific inflammatory osteoclast precursors induced during chronic inflammation give rise to highly active osteoclasts associated with inflammatory bone loss, Bone Res. 10 (2022).
[71] J. Brinkmann, T. Hefti, F. Schlottig, N.D. Spencer, H. Hall, Response of osteoclasts to titanium surfaces with increasing surface roughness: an in vitro study, Biointerphases 7 (2012) 1–9.
[72] S. Makihira, Y. Mine, E. Kosaka, H. Nikawa, Titanium surface roughness accelerates RANKL-dependent differentiation in the osteoclast precursor cell line, RAW264.7, Dent. Mater. J. 26 (2007) 739–745.
[73] N.L. Davison, et al., Submicron-scale surface architecture of tricalcium phosphate directs osteogenesis in vitro and in vivo, Eur. Cell. Mater. 27 (2014) 281–297.
[74] A.H. Mohammed Mohammed, K.A. Shariff, M.H.A. Bakar, H. Mohamad, A review on the behavioral responses of osteoclast and osteoblast cells on the near-surface of the bioceramic coating: roles of ions released, solubility, and pH, J. Aust. Ceram. Soc. 58 (2022) 1715–1727, 2022 58:5.